Peer-reviewed version available at *Polymers* **2020**, *12*, 439; doi:10.3390/polym12020439

# Covalent Surface Functionalization of Bovine Serum Albumin to Magnesium Surface: Enhancing Robust Corrosion Inhibition and In vitro Osteo-inductivity

Seo Yeon Lee [a], Sita Shrestha [a], Bishnu Kumar Shrestha [*, a], Chan Hee Park [*, a, b], and Cheol sang Kim [* a, b]

[a]Deparment of Bionanosystem Engineering, Graduate School, Jeonbuk National University, Jeonju 561-756, Republic of Korea

[b]Division of Mechanical Design Engineering, Jeonbuk National University, Jeonju 561-756, Republic of Korea

---

* Authors to whom correspondence should be addressed.

E-mail: chskim@jbnu.ac.kr, biochan@jbnu.ac.kr, bishnuaampipal@hotmail.com, Tel.: +82 63 270 4284, Fax: +82 63 219- 5294

Peer-reviewed version available at *Polymers* **2020**, *12*, 439; doi:10.3390/polym12020439

**Abstract**

Herein, we describe precisely on covalent modification of pure magnesium (Mg) surface and applied to induce *in vitro* osteogenic differentiation. A new concept, chemical bonding method is proposed for developing stable chemical bonds on Mg surface through serial assembly of bioactive additives including ascorbic acid (AA) and bovine serum albumin (BSA). The coating with such potential materials shows strong integrity to the Mg and could suitable for cell-interface interaction with the host tissue during implantation in bone tissue repair. The physicochemical and electrochemical properties of surface modified Mg assess how these nanoscales layered of biomolecules could demonstrate the significance improvement in chemical stability of coating. The modified Mg-OH-AA-BSA exhibits better anti-corrosion behavior with high corrosion potential ($E_{corr}$ ~ – 0.96 V) and low corrosion current density ($I_{corr}$ ~ 0.2 µA $cm^{-2}$) as compared to pure Mg ($E_{corr}$ ~ –1.46 V, $I_{corr}$ ~ 10.42 µA $cm^{-2}$). Outer layer of BSA on Mg protects fast degradation rate of Mg which is the consequence of strong chemicals bonds between amine groups on BSA with carboxylic groups on AA. Collectively, the results suggest that surface modified Mg provides strong bio-interface and enhances the proliferation and differentiation of pre-osteoblast (MC3T3-E1) cells through protein-lipid interaction. Owing to this fact, the cost-effective and scalable covalent functionalization of Mg surface inherits biological advantage in orthopedic and dental implants with long term stability.

Keywords: Magnesium; Covalent bonds; anti-Corrosion; biocompatibility; Bovin serum albumin

## 1. Introduction

The implantable scaffolds that can inherit a remarkable biological and physiological bio-interface to host stem cells are rapidly expanding their applications towards clinical studies in bone tissue engineering [1, 2]. Such scaffolds have tendency to acquire biomimetic behavior akin to those of native host tissue for absorbing proteins, biominerals and interacting with extracellular matrix (ECM)[3]. Importantly, the biomimetic scaffolds are liable to complement in wound healing system or tissue engineering which leads to restore tissue functions, enhance stem/progenitor cells regeneration, and regulate the delivery of the cells growth factors and cytokines [4]. The principal determinants of biomedical implants to their functional success basically depend on biocompatibility, natural integrity with host tissue and bioresorbable [5]. In bone tissue or hard tissue engineering, the strong mechanically behavior, osteoinductive, osteoconductive, immunocompatible and fast-corrosion resistance with long-term stability are crucial properties in the level of artificial graft level [6, 7]. Various materials including metals and their alloys, natural and synthetic polymers in two dimensional (2D) and three dimensional (3D) structural framework in the form of nanofibers, and hydrogels in hybrid nanostructured confer physicochemical and biological substitute in bone tissue repair [8-11].

A common interest to engineer biologically active and load bearing scaffolds have been explored extensively which can be tailored to provide suitable structural framework for supporting cellular attachment leading to cell differentiation and tissue formation [12, 13]. Fortunately, to study on magnesium strides in bone tissue engineering application can be associated with the lightest structural metal, biodegradable, recyclable and biocompatible [14, 15]. These properties furnish Mg highly attractive for orthopedic implantable device for fracture repair with substantial capabilities to improve regeneration and reconstruction of bone tissue by preventing implant

loosening, potential infection, morbidity in the vicinity of the implantable site and premature failure after surgery [16]. However, fast degradation or increase in corrosion rate and presumably hydrogen production from pure magnesium and its alloys *in vivo* do not provide prolonged mechanical support along with increase in alkalinity after surgical procedure as a consequence failing of bone-fracture healing [17]. Over the past several years, an extensive efforts and approaches have been employed to overcome the number of inherent limitations concerned to Mg and its alloys including rapid corrosion that trigger to challenge for orthopedic, dental and prosthetic applications [18-20]. The treatment of Mg surface to obtain Mg scaffolds with osteo-friendly biomimetic materials including β-tricalcium phosphate (β-TCP) hydroxyapatite (HA) chitosan through dip casting and immersion methods has been studied for enhancing osteogenesis and osteoimmuno-modulatory behavior [21, 22]. The supplementation of these materials is known to be beneficial to people with osteoporosis. However, such traditional approaches are still in noticed which unable to improve effective anti-corrosion behavior of surface modified Mg and its alloy. Furthermore, various techniques, such as plasma spraying, sol-gel coating, electrophoretic deposition, sputter deposition and spin coating were devoted using foreign metal oxide or particles (silica titanium, zirconium, aluminum) on magnesium surface to improve corrosion resistance behavior[23, 24]. But the low chemical stability, poor ionic conductivity, non-uniform shape and size, accumulation of nanoparticles, and biodegradation assist for possible release of metallic nanoparticles/ ions in cellular environment affect the proliferation and differentiation of stem cells which lead to poor stimulation on cellular activity, intracellular changes such as disruption of cellular metabolism and organelles integrity that rise to expect gene alternation [25, 26]. Moreover, synthetic polymers such as polycarpolactone (PCL), poly (lactic-co-glycolic acid (PLGA) polylactic acid (PLA) were coated on Mg surface through layer-by-layer or multilayers system to

improve its biocompatibility and anti-corrosion behavior but there exist some limitations including, easily peel off from the Mg surface due to only physical attachment, high cost of materials, and more hydrophobic membranes which causes very slow diffusion of ECM and other biomolecules through implant interfacial microstructure as a result retardation the ability of cells attachment, proliferation and cellular activities during *in vitro* and *in vivo* application [27, 28].

Here, we report the potential application of surface modified magnesium for in vitro bioimplant in bone tissue engineering using MC3T3-E1 as model cells instead of using Mg alloy. A simple, and cost-effective chemical modification method was applied to generate ample of reactive chemical moieties susceptible to form strong covalent bonds on Mg surface. The surface functionalized Mg (Mg-OH-AA-BSA) via successive treatments of ascorbic acid followed by bovine serum albumin was confirmed by comprehensive results to ensure strong anti-corrosion behavior, surface controlled biological fixation of biomolecules or proteins alongside long-term physiological stability, and robust performance to promotes osteoblastic differentiation.

## 2. Experimental section

### 2.1 Materials

Two pure magnesium rods of diameter 12.7 mm and 7.9 mm (purity ~ 99.9%), sodium hydroxide (NaOH), and L-Ascorbic acid ($C_6H_8O_6$, mw ~ 176.12, > 99.0%) were purchased from Sigma-Aldrich, Korea. Bovine serum albumin Fraction V (Roche Diagnostics GmbH, Mannheim, Germany) was obtained for surface treatment of Mg. The simulated body fluid (SBF) solution was prepared in accordance to the previously reported literature [29]. Regents in aqueous solution were prepared in ultra-pure water obtained from a Millipore-Q-system. All of the chemicals and reagents were of analytical grade and used as received without any further purification.

### 2.2. Sample preparation

The Mg rod of diameter 12.0 mm and height 5.0 mm was taken for the successive surface modification called as surface chemical treatment. Prior to the chemical treatments, the surface of each Mg specimen was ground successively to 400, 800, 1200, and 2000 grits (SiC) and washed, followed by ultrasonic bath in ethanol for 10 min in each step to remove any remaining residue from the Mg surface and dried on nitrogen atmosphere for 4 hours. The surface modification of Mg is illustrated through the schematic 1. Briefly, the pure Mg was first treated with 5.0 M NaOH in aqueous solution for 48 hours at 60 ℃ to generate large number of hydroxyl (-OH) groups on the Mg surface in associated with the passivation. Then, it was taken out from the solution and washed several times with DI water. The dried Mg-OH sample was treated with 0.02 M AA for 24 hours at 37 ℃ prepared in ethanol. The treatment of AA with Mg-OH induces adequate chemical bonding through -OH and -COOH bonds in order to form protective layers. Subsequently, the AA treated Mg substrate was further immersed into 0.5 mM BSA for 48 hours at 37 ℃. The BSA forms strong bonds through -$NH_2$ groups and hydrogen bonds, as a consequence the Mg reduces the ability of fast corrosion rate. This aspect has made Mg-OH-AA-BSA ideal candidate for the most biocompatible, highly protective multi layers structure and capabilities that enable substantial enhancement of anti-corrosion behavior and lead to their extensive study in biomedical application. Similar processes were employed for the surface modification of pure Mg with dimension 1.0 cm (diameter) and 0.5 cm (height) to evaluate the hydrogen evaluation test.

### 2.3. Materials Characterization

#### 2.3.1. Physical characterization

The surface morphologies of pure and treated Mg samples were observed by field-emission scanning electron microscopy (FE-SEM, Carl Zeiss Supra - 40 VP, Germany). The crystallinity of

the samples was characterized using X-ray diffraction (XRD, Rigaku Japan) with Cu Kα (λ=1.542 Å) radiation over a range of Bragg angle (2θ) of 10°–90°. Newly formed bonds were also confirmed by Fourier Transmission Infrared Spectra (FT-IR) using Perkin Elmer Spectrum GX, USA). Atomic Force Microscope analysis (AFM, Multimode 8, Bruker) was conducted to evaluate the surface roughness of the sample before and after the potentiodynamic corrosion test. Water contact angle (WCA) was measured on water contact angle meter (GBX-Digidrop, France) at room temperature (RT) in static drop methods, where distilled water of 5 µL droplet was dropped on the surface of each sample and the angle was measured at 1, 3 and 5 seconds.

### 2.3.2. Electrochemical measurement

Electrochemical analysis such as, determination of open circuit potential (OCP) *vs*. time, potentiodynamic polarization test, and electrochemical impedance spectroscopy were conducted using ZIVE SP1 Potentiostat/Galvanostat/EIS electrochemical analyzer (WonATech Co. Ltd. Seoul, Korea) to determine the OCP of the cell running for 30 min, corrosion resistance behavior of prepared magnesium samples and charge transfer property of the samples respectively. We used three-electrode electrochemical configuration, where Mg or modified Mg samples were used as working electrodes, saturated calomel electrode (SCE) as reference electrode and platinum mesh as counter electrode. Inorganic salts of magnesium sulfate, calcium chloride and sodium bicarbonate along with Hank's balanced salts (H2387, Sigma Aldrich, Korea) were dissolved in one liter DI water (pH 7.4) in accordance to the literature [30] and the solution- simulated body fluid (SBF) was used as electrolyte for each electrochemical measurement at RT. The potentiostatic electrochemical impedance spectroscopy (EIS) was recorded from all surface modified and pure Mg in SBF solution (pH 7.4) at an amplitude of 10 mV and zero bias potential

in a frequency range from 100 kHz to 1 mHz. All samples were stabilized in SBF for 1h 30 min at 37 ℃ and the electrolyte was also purged with pure nitrogen ($N_2$) for 15 min to reduce the oxygen that dissolved on the electrolyte before each measurement. The corrosion potential was measured via Tafel extrapolation polarization from potential scanning from ─ 2 V to zero *vs.* OCP at constant sweep rate of 1 mV/s. All the samples with effective interface surface area of 0.875 $cm^2$ were examined for their electrochemical study.

**2.3.3. Hydrogen evolution test**

The corrosion behavior of as-prepared samples was evaluated through the conventional immersion test method. The volume of hydrogen ($H_2$) evolved at different point times was measured and the degradation rate ($DR$) was calculated at normal temperature and pressure (NTP) using the relation, $(\mathrm{DR}) = \frac{PV}{RT}\left(\frac{M}{At}\right)$, where 'P,V,R,T,M, A, and t' correspond to normal pressure at RT, volume of $H_2$ evolved in mL, universal gas constant, RT in kelvin, molar mass of Mg, active surface area, and exposure time respectively [31]. The process was carried out at different time points to monitor the degradation of magnesium. Each tested sample (n=3) was separately immersed into air tight system using eudiometer containing 500 ml SBF and then incubated at 37 °C for a total of 8 days. The volume of $H_2$ from each sample was measured every 12 h difference (i.e. 6 and 12 h, and 24h, 36, up to 192 h). The corrosion rate was calculated on the last 24 h of $8^{th}$ day. Pure Mg with dimension 1.0 cm (diameter) and 0.5 cm (height) was taken as reference sample.

**2.3.4. *In vitro* cells interaction**

pre-osteoblasts (MC3T3-E1) cells line derived from mouse Clone 4, ATCC CRL-5293 were first cultured in Minimum Essential Medium (a-MEM, Gibco™, ThermoFisher Scientific) under incubation at 37 °C and 5% carbon dioxide ($CO_2$) in accordance to the previously reported literature [32, 33]. Briefly, cells at almost 85 % confluency were harvested then seeded onto the

center of sterile (under UV light for over-night) tissue culture plate and Mg-OH-AA-BSA scaffold at a density of $3\times10^4$ cells/well. The cells were cultured for different time points (for example 1, 3, and 7 days). During this time the cell medium was replaced every second day. Furthermore, cell viability test was conducted to evaluate the cells proliferation, survivability and cytocompatibility on the as-prepared scaffolds and were continually monitored up to 7-day period using the cell counting kit-8 (CCK-8) at interval of 1, 3 and 7-days of cell culture. At preferred time points, the CCK-8 test solution was added to each 24-well plate and was incubated for 2 h at 37 °C incubator with 5 % $CO_2$. The measurement of the absorbance was checked at 450 nm using a microplate reader (Tecan, Austria) in 96 well plate.

### 2.3.5. Cell morphology observation

The morphological study of the MC3T3-El cells grown *in vitro* were evaluated by fixing the cells with 4 % glutaraldehyde solution for an hour on days 1, 3, and 7 post seeding followed by washing with PBS to remove the non-adherent cells. Again, washed with PBS followed by dehydrated in a graded series of ethanol concentration (20 %, 30 %, 50 %, 70 %, and 100 %) for 10 min each. The cell samples were dried for 12 h in clean bench before observing cells morphology by using cell scanning microscopy at different magnification (JSM-6400 JEO, Japan). In addition, to obtain the confocal images, the cells cultured on the Mg-OH-AA-BSA scaffolds were washed with PBS after aspiration of media from 24-well plate. The cells were fixed with 4 % paraformaldehyde for 10 min at RT and permeabilized in 0.2 % triton (X-100) for 2 min. The cells were blocked with 1 % human serum albumin for 30 min. The scaffolds attached with cell were consecutively stained by Rhodamine-phalloidin for cytoplasm (20 min), and DAPI for cell nuclei (5 min), at RT in dark condition followed by washing with PBS. The fluorescence images of the cells were taken using a confocal microscopy (Zeiss LSM 800 Airyscan, Carl Zeiss Micro imaging Inc., NY, USA).

### 2.3.6. Statistical analysis

Data were evaluated using One-way analysis of variance (ANOVA) followed by post-hoc Tukey comparison test at a 95 % confidence level and presented as mean ± standard deviation (SD, n=3). Statistical significance was considered when *$p<0.05$, and ***$p<0.001$.

## 3. Results and discussion

### 3.1. Surface morphology analysis of coating

The surface topography of magnesium substrates with multilayer coating of chemical moieties including ascorbic acid and BSA were studied through FE-SEM images in Fig.1. before emersion in to SBF solution. A smooth and shining surface was observed on of pure Mg (Fig1. (a)) due to its high crystallinity. When the surface of Mg samples was coated or treated successively through layer-by-layer technique in accordance to the formation of strong chemical bonding with NaOH, AA and BSA (Fig.1, c-d) the surface roughness slightly increased. The nanoscale of BSA layer on the outer surface made the surface more smoothness as compared to Mg-OH and Mg-OH-AA surface confirming the hydrophobic protein layers was strongly attached on the Mg modified surface. Figure 2. shows the surface corrosion morphologies of Mg and Mg modified samples after immersion in SBF for 2 hours followed by potentiodynamic corrosion test. Pure Mg has large microcracks with increase in surface roughness due to its high reactivity but the passivation of Mg increase after treating with NaOH. The electrovalent bonding between Mg with hydroxyl groups decrease the reactivity into aqueous phase and relatively lower cracks were obtained (Fig.2. b). Additionally, the Mg-OH surface covered with AA groups reduced furthermore the microcracks. It is obvious that the formation of several chemical bonds including covalent and hydrogen bonds between Mg-OH and AA leading the Mg -OH-AA less sensitivity to pitting corrosion resulted

considerable increase in surface smooth (Fig.2, (c)). Importantly, we have been focusing to prepare improved anti-corrosion property of Mg and it is expected with the surface modification of Mg -OH-AA with treated with BSA. The Mg-OH-AA-BSA (Fig.2, (d)) modified sample showed significant improved in surface smoothness as compared to others. The surface morphology changed remarkably with very less in cracks in whole surface and exhibited chemical inertness which are as consequences of strong -OH, -COOH, $-NH_2$ and hydrogen bonds between BSA to AA. In addition, our AF microscopy results in Fig.3. confirm that the average surface roughness (Ra ~114 nm) value and Rq (~ 145 nm) value in the two-dimensional (2D) and three-dimensional (3D) micro/nano structure of Mg-OH-AA-BSA has almost ~3-folds less than the pure Mg, which indicates that the BSA modified Mg has uniform and smooth surface after the strong encapsulation by BSA. This suggests that the appropriate roughness on Mg-OH-AA-BSA sample surface could exhibit preferentially for stem cells functions and adsorption of protein/lipid or extracellular matrix (ECM) through polar interactions.

The XRD patterns of the as-prepared materials are shown in Fig.4 (a). The hexagonal phase crystallography of pure Mg was confirmed from the diffraction peaks profiles in several lattice planes (100, 002, 101, 102, 110, and 200) corresponding to $2\theta$ = 32.61, 34.89, 37.19, 48.25, 57.87, and 67.62) degree respectively. These values are in consistence to the values reported previously in literature [34]. This values in degree in associated with planes indicate the purity of Mg without presence of oxide and hydroxide layers on Mg surface. However, no notable peaks were observed on Mg $(OH)_2$ but the multiple diffraction peaks appeared from Mg $(OH)_2$ also in agreement with the hexagonal structure of Mg $(OH)_2$ (JCPDS 7-239). The successive surface modification of Mg by AA followed by BSA has no significant effects on its crystallography. Interestingly, the peaks intensities are decreased in the modified Mg in respect to the presence of nanoscale layers of BSA

strongly coated on Mg surface. Furthermore, the FT-IR spectroscopy analysis depicted in Fig. 4 (b) describes the adsorption peaks at different frequency region in the range from 800 $cm^{-1}$ to 3700 $cm^{-1}$. The absorption peak at around 862 $cm^{-1}$ is assigned to Mg-O bonds in vibrational mode. A notable peak appeared at 1470 $cm^{-1}$ may be the presence of Mg-H bonds. It might have been be possible that after treatment of Mg in strong alkaline solution (sodium hydroxide) at high temperature (~ 80°C), the $Mg^{++}$ ions at the surface of Mg can combine with hydride ($H^-$) ions (produce from oxidation of sodium hydroxide) as a result new Mg-H bond is formed. In addition, the adsorption band at 1053 $cm^{-1}$ and 3700 $cm^{-1}$ correspond to the formation of Mg-O and Mg-OH respectively [35]. But a well-defined bands are appeared at 1074 $cm^{-1}$,1364 $cm^{-1}$and 1618 $cm^{-1}$ confirms the C-O-C, enol-hydroxyl groups, and C=C respectively from ascorbic acid on Mg surface [36]. It is worth noting that a wide band intensity around at 3359 $cm^{-1}$ indicates the presence of -OH in AA that bonded to Mg-OH through ample of hydrogen bonds. We further confirmed that the conjugation of BSA to AA modified Mg through the strong adsorption band of BSA on Mg surface. The characteristic bands of BSA at 1385 $cm^{-1}$, 1527 $cm^{-1}$ and 1654 $cm^{-1}$ are attributed to C-N stretching, N-H bending mode of amide II and C=O stretching mode of amide I respectively [37]. These particular bands intensities present in Mg-OH-AA-BSA substrate indicate the nanoscale layer of BSA uniformly encapsulated to Mg surface through strong $-NH_2$, C=O and covalent bonds.

To investigate the surface interface of as-prepared Mg samples with water molecule, we performed static water contact angle measurement as shown in Fig.5 Pure Mg exhibited lower WCA value (~ 32.2 º) as compared to the WCA value of Mg-OH (~ 45.5 º), and Mg-OH-AA (~39.7 º). It is most important that the ample of oxide layers on reactive Mg at RT are susceptible to form H bonding with $H_2O$. However, the -OH moieties on Mg-OH, and Mg-OH-AA layer makes the modified

samples more passivate than pure Mg for the formation of H bonding. Consequently, the increased in water contact angle were observed on Mg-OH, and Mg-OH-AA. In addition, the effective WCA was examined on surfactant-bonded BSA (protein) on Mg surface. As we know that BSA, an amphiphilic nature, absorbs $H_2O$ forcefully and reduce the interfacial tension by immobilized with in the water. Thus, the hydrophobic interaction increases on BSA modified Mg (Fig.5. (d), is confirmed from the value of WCA on Mg-OH-AA-BSA (~ 75.8 º). It is obvious that the hydrophobic proteins have great extent for their stability, and biological function as nonpolar interaction with ECM, which helps to bind more other lipids and proteins [38]. Such materials have more advantageous towards cytocompatibility and could be preciously applicable for the development of bioimplant in hard tissue engineering.

The volume of hydrogen evolved from the Mg samples measured and was expressed in Fig.6. The curve (d) depicts that no $H_2$ was evolved till 60 h form Mg-OH-AA-BSA sample. However, at the end of 3$^{rd}$ day, the degradation rate on the basis of $H_2$ evolution was calculated and found to be 2.7 mg cm$^{-2}$ day$^{-1}$ in pure Mg. In contrast, the surface modified Mg samples showed gradually lower degradation rates and basically the Mg-OH-AA-BSA has significantly the lowest corrosion rate (0.04 mg /cm$^2$.day) indicating that the nanolayer of BSA has strongly protected the Mg surface through effective chemical bonding to inter molecular chemical moieties. At the 8$^{th}$ day, the BSA modified showed little increases in corrosion rate (2.7 mg cm$^{-2}$ day$^{-1}$) as compared to 3$^{rd}$ day. The increased in corrosion rate might have been the consequence of small pit formed on Mg so that the release of metal ions increased from the mechanism chemical degradation reaction given by: $Mg + H_2O \rightarrow Mg^{2+} OH^{-} + H_2\uparrow$. The pure Mg released more Mg ions in SBF solution but suppressed on Mg-OH-AA-BSA, which is only caused by the compact layer of BSA exhibiting physical and chemical stability [39].

### 3.2. Electrochemical study

First, to evaluate how the chemical moieties linked with BSA influence the anti-corrosion performance of Mg samples, we choose all surface modified Mg including pure Mg for OPC measurement in Fig.7. (a). Chemically, the outer surface of modified Mg-OH-AA-BSA is composed of multiple functional (-OH, -$NH_2$, and -COOH) groups associated with ample of inner and inter ionic bonding and other bonds (for examples of hydrogen bonding, amide-hydrogen bonding). These interconnected molecules forming layered-like structure on Mg surface. The samples with different layered structure showed variable OCP of the cell. The OCP (vs. time) results from the different samples illustrate that the Mg has lower cathodic potential, while the anodic potential gradually increased and Mg-OH-AA-BSA has stable and the largest anodic potential. The decrease in cathodic potential shown by Mg (~ -1.45 V) is ascribed to the faster in dissolution of active bare Mg. It is worthy mention here that the higher in anodic potential exhibited by Mg-OH-AA-BSA around ~ -1.1 V is the lowest OCP value of the running cell ever till now than the previously reported literatures [40, 41]. The uniform coating of BSA has a potential advantage to suppress the corrosion reaction and reduces the $H_2$ evolution rate. This result indicates that, under such chemical modification, the anti-corrosion behavior of Mg-OH-AA-BSA showed much better performance than that of other commonly employed methods [42].

The potentiodynamic polarization curves obtained from the different samples were expressed in Fig.7(b). The Mg-OH-AA-BSA showed the highest corrosion potential ($E_{corr}$) value along with the lowest corrosion current density ($I_{corr}$). The electrochemical corrosion parameters determined from Tafel slop extrapolation are listed on Table 1. The free corrosion potential of the surface modified Mg including pure Mg showed in the order of Mg < Mg-OH< Mg-OH-AA < Mg-OH-AA-BSA. In contrast, the $I_{corr}$ form the samples are in reversed order. This indicates that the

formation of chemical bonds after consecutive modification of Mg surface enhanced the electrochemical stability in Mg-OH-AA-BSA. Meanwhile, the more negative value of $I_{corr}$ in BSA modified Mg showed the best anti-corrosion property, which is attributed to the strong protective layer of BSA. In general, proteins interact with metals through adsorption and chelation and improves the anti-corrosion behavior. However, BSA has no ability to protect the anti-corrosion behavior of first row d-block metals due to its ability to form complexes and can occurs dissolution of metals by protein catalyzed reaction [43] but formation of oxide and hydrate layers in Mg surface enhance the bond strength with BSA. Consequently, both the cathodic reaction of hydrogen evolution and dissolution of $Mg^{2+}$ (anodic oxidation) can be significantly reduced. In addition, the Mg-OH-AA-BSA showed almost no pitting potential as compared to other modified samples including pure Mg. The result obviously confirms that the chemical modification of Mg surface through the formation of covalent bonds, amine bonds, and hydrogen bonds has true and stable modification technique and was proved by the remarkably higher cathodic potential (-0.96 V) value of Mg-OH-AA-BSA. Moreover, the inhibition efficiency η (%) of the BSA modified Mg was calculated and found to be 98.08 % indicating to suppress the cathodic electrochemical corrosion behavior which is also in agreement to the FESEM images (Fig.2d). Moreover, the $E_{corr}$ and $I_{corr}$ observed on Mg-OH-AA-BSA (n=3) showed almost 97.23% reproducibility indicating the good reproducibility of the prepared samples (Fig.7d).

Figure 8. depicts the Nyquist and Bode plots in order to evaluate the electrode/electrolyte interface in potentiodynamic polarization reaction that occur at electrode surface in SBF solution. The Nyquist plots illustrate that the chemical modification of Mg-OH and Mg-OH-AA showed larger impedance than pure Mg. This result clarifies the formation of protective layers of oxide and hydration in associated with carboxylate groups can passivate the coating layers. Importantly,

chelating behavior of BSA resist to percolate the electrolytes during cathodic polarization reaction and increased the impedance behavior significantly. The excessive large capacitive loop (Fig.8 b) exhibited by Mg-OH-AA-BSA substrate corresponds to charge transfer resistance ($R_{ct}$) at higher frequency region indicates the best agreement to theoretical hypothesis, suggesting a better anti-corrosion chemical modification compared to only oxide and hydrate layer coating layers on other samples. The chemically modified Mg-OH and Mg-OH-AA (Fig. 8 (c) and (d)) showed higher impedance modulus value than bare Mg but the value appears remarkably higher on Mg-OH-AA-BSA due to organic barrier of proteins. The corrosion processes were further elaborated through the equivalent electrical circuits (ECs) in insets Figs. 6 to determine the impedance parameters in circuits. The ECs as shown in inset Fig. 8 (c) represent for three samples (Pure Mg, Mg-OH, and Mg-OH-AA) as in the model: Rs-Qdl|$R_{ct}$-Qp|Rp, and for Mg-OH-AA-BSA was proposed as Rs-(Qdl|Rp)|$R_{ct}$-w, where Rs represent the resistance from electrolytes, Qdl and $R_{et}$ double layer capacitance and charge transfer resistance respectively. Similarly, $Q_p$ is capacitance due to the natural oxide in surface, $R_p$ relate to the resistance attributed during charge transfer reaction and w represents the Warburg impedance [43]. Moreover, phase angle diagram of Mg-OH-AA-BSA in Fig.8(f) approaching around -89.23º at medium range frequency which is significantly lower as compared to other samples. This is results verify the passivation of outermost layer of materials causing the synergetic effete of oxide film covalently bonded to proteins forming protective layer [44].

Table.1 The value of electrochemical parameters obtained from various samples using potentiodynamic polarization technique, (calculated from Tafel plots and Nyquist plot) measured in SBF solution at 37℃.

| Samples | Polarization parameters | | | Nyquist Plots | | | | |
|---|---|---|---|---|---|---|---|---|
| | Ecorr *Vs.*(SCE) | $I_{corr}$ ($\mu A.cm^2$) | $-\beta_c$ (mV/dec) | Rs ($k\Omega.\ cm^2$) | Rct ($K\ \Omega.\ cm^2$) | Rp ($K\ \Omega.\ cm^2$) | Qdl ($\mu F.cm^{-2}$) | Qp ($\mu F.cm^{-2}$) |
| Pure Mg | -1.46 | 10.42 | 0.108 | 0.26 | 0.012 | 0.014 | 62.43 | 8 |
| Mg-OH | -1.43 | 1.04 | 0.148 | 0.24 | 0.051 | 0.049 | 3.41 | 5.26 |
| Mg-OH-AA | -1.34 | 0.61 | 0.135 | 0.23 | 0.11 | 0.068 | 1.62 | 2.1 |
| Mg-OH-AA-BSA | -0.96 | 0.20 | 0.274 | 11.66 | 344.52 | 283.51 | — | — |

‡ 1.951 $e^{-7}$ ($\Omega$) Warburg constant of Mg-OH-AA-BSA sample.

### 3.3 In vitro cell viability

Pure Mg sample is inappropriate for long time direct integration with stem cell during *in vitro* cell viability test due to its rapid corrosion rate [7]. Thus, not suitable for considering biomedical implant. In this work, a comparative analysis was conducted to evaluate the osteogenic activity of Mg-OH-AA-BSA sample in MC3T3-E1 cells through CCK-8 test result (Figure 9 (a)). The development and proliferation of the cells on as-prepared samples were observed at different time points, where the cell viability on the samples did not show more significant different as compared to cell grown on tissue culture plate (TCP, taken as control group). The formation of oxide layers on Mg surface associated with chemical bonding of other multi-functional groups ($NH_2$, COOH, -OH) via layer-by-layer modification method lead to introduce a nanoscale layer of proteins (BSA) easily, which promote osteogenic properties existing natural environment on Mg-OH-AA-BSA. The protein-based scaffolds have osteoinductive ability that is essential for tissue regeneration. The cells were significantly less proliferated on Mg-OH-AA-BSA than TCP on 1 day. In the first 24 h, the cells were unable to adopt sufficiently into the protein rich scaffold due to the changing

functional moieties on scaffolds-cell interface interaction. However, the anabolic activities were gradually increased on the scaffolds and the scaffold promoted the growth and proliferation of MC3T3-E1 cells on both 3 and 7 days. The outer layer of BSA on the scaffolds provides nutrients easily that bonded on protein. The regular intake of proteins stimulate the bone cells formation along with differentiation and assist to suppress bone breakdown [45]. It is noteworthy to mention here that the Mg-OH-AA-BSA scaffold with sufficient protein provides natural environment and have great impacts for cell functions. It was confirmed from comparative study of cell proliferation rate occurred on the scaffolds and the TCP. In addition, the significant improvement (***$p > 0.001$) of cell growth and proliferation observed on the scaffolds on 3 and 7 days supports the evidence of strong protective layer and anti-corrosion behavior of BSA modified scaffolds. The cells remarkably proliferated the scaffolds (*$P < 0.05$) than on TCP indicating that the as-prepared Mg-OH-AA-BSA scaffold demonstrate potential effect for *in vitro* cell adhesion, growth, and proliferation. This results prevalence the implication of the scaffolds for long term bioimplant in association with perfect remodeling of bone cells.

Figures 9 (b-d) and 10. show the cell scanning microscopy images and confocal fluorescence images of preosteoblast cells after culturing on the Mg-OH-AA-BSA scaffold at three different time points respectively. The cells attachment, growth, and proliferation gradually improved with prolonged period of time up to 7 days. The cells were uniformly distributed with high confluency rate at 7 days, indicating the uniform coating of BSA on the surface modified Mg enhanced the development of cells. The cellular morphology on the scaffold at day 3 clearly shows that the cells are spreading naturally and strongly attached on the scaffold than 1 day (Figs. 9 b and c). Furthermore, the Fig. 9 (d) displays the high cell density with good cell proliferation suggesting that the scaffold exhibited better biocompatibility, and strong anti-corrosion behavior. The

adhesion, distribution and proliferation of the cells represented by the fluorescence images (Fig. 10) are also in agreement with the SEM images (Figs. 9(c-d)). Here, it is clear that the chemically modified Mg surface with protein rich protective layer provides sufficient nutrients for the cells and the cells functions (for example, growth and differentiation) remarkably enhanced. Such results are the clue for the application of Mg-OH-AA-BSA bio implant bone formation.

## 4. Conclusion

In summary, we controlled the fast-biodegradable property of Mg via covalent functionalization on its surface along with the formation of nanoscale layer of BSA. The electrochemical behavior of the Mg-OH-AA-BSA substrate reveals that the formation of covalent bonds through successive addition of functional moieties on Mg surface to prevent fast corrosion rate of Mg. The modified Mg-OH-AA-BSA substrate showed surface smoothness and strong anti-corrosion behavior indicating perfect coating of BSA. The surface WCA of Mg-OH-AA-BSA sample exhibited hydrophobic character, which is beneficial for the protein-protein or protein-lipid interactions. In addition, the uniform coating of protein on the surface creates the natural environment for the development and proliferation of MC3T3-E1 cells. The Mg-OH-AA-BSA showed good osteo-compatibility and osteo-integrative performance to MC3T3-E1 cells. The facile novel idea could apply for the modification of light weigh metal and has potential efficacy for the fabrication of bio implant devices for bone tissue application.

## Acknowledgements

The authors are highly grateful for the financial support from the Basic Science Research Program through National Research Foundation of Korea (NRF) by Ministry of Education, Science and Technology

(Project no. 2018R1D1A1B07044717) and also grant from 2018 R&D Special Zone Development Project technology transfer project 2018DDRD011201201.

## References

1. Vapniarsky, N., et al., *Tissue engineering toward temporomandibular joint disc regeneration.* Science Translational Medicine, 2018. **10**(446).
2. Wong, H.M., et al., *In vivo stimulation of bone formation by aluminum and oxygen plasma surface-modified magnesium implants.* Biomaterials, 2013. **34**(38): p. 9863-9876.
3. Aslankoohi, N., et al., *Bone Repair and Regenerative Biomaterials: Towards Recapitulating the Microenvironment.* 2019. **11**(9): p. 1437.
4. SJ, H., et al., *Engineering craniofacial scaffolds.* Orthodontics & Craniofacial Research, 2005. **8**(3): p. 162-173.
5. Li, L., et al., *Design and Biophysical Characterization of Poly (l-Lactic) Acid Microcarriers with and without Modification of Chitosan and Nanohydroxyapatite.* 2018. **10**(10): p. 1061.
6. Yaszemski, M.J., et al., *Evolution of bone transplantation: molecular, cellular and tissue strategies to engineer human bone.* Biomaterials, 1996. **17**(2): p. 175-185.
7. Shah, N.J., et al., *Surface-Mediated Bone Tissue Morphogenesis from Tunable Nanolayered Implant Coatings.* Science Translational Medicine, 2013. **5**(191): p. 191ra83-191ra83.
8. Atala, A., F.K. Kasper, and A.G. Mikos, *Engineering Complex Tissues.* Science Translational Medicine, 2012. **4**(160): p. 160rv12-160rv12.
9. Liu, M., et al., *Injectable hydrogels for cartilage and bone tissue engineering.* Bone Research, 2017. **5**: p. 17014.
10. Shrestha, B.K., et al., *Development of polyamide-6,6/chitosan electrospun hybrid nanofibrous scaffolds for tissue engineering application.* Carbohydrate Polymers, 2016. **148**: p. 107-114.
11. Shrestha, S., et al., *A conducting neural interface of polyurethane/silk-functionalized multiwall carbon nanotubes with enhanced mechanical strength for neuroregeneration.* Materials Science and Engineering: C, 2019. **102**: p. 511-523.
12. Fong, E.L.S., et al., *Building Bridges: Leveraging Interdisciplinary Collaborations in the Development of Biomaterials to Meet Clinical Needs.* Advanced materials (Deerfield Beach, Fla.), 2012. **24**(36): p. 4995-5013.
13. Vidal, G., et al., *Enhanced cellular adhesion on titanium by silk functionalized with titanium binding and RGD peptides.* Acta Biomaterialia, 2013. **9**(1): p. 4935-4943.
14. Bose, S., M. Roy, and A. Bandyopadhyay, *Recent advances in bone tissue engineering scaffolds.* Trends in biotechnology, 2012. **30**(10): p. 546-554.
15. F., W., et al., *Biodegradable magnesium scaffolds: Part 1: Appropriate inflammatory response.* Journal of Biomedical Materials Research Part A, 2007. **81A**(3): p. 748-756.
16. Farraro, K.F., et al., *Revolutionizing orthopaedic biomaterials: The potential of biodegradable and bioresorbable magnesium-based materials for functional tissue engineering.* Journal of biomechanics, 2014. **47**(9): p. 1979-1986.
17. Esmaily, M., et al., *Fundamentals and advances in magnesium alloy corrosion.* Progress in Materials Science, 2017. **89**: p. 92-193.
18. Zhang, Y., et al., *Implant-derived magnesium induces local neuronal production of CGRP to improve bone-fracture healing in rats.* Nature Medicine, 2016. **22**: p. 1160.

19. D., K.H., et al., *Biomimetic Materials and Fabrication Approaches for Bone Tissue Engineering.* Advanced Healthcare Materials, 2017. **6**(23): p. 1700612.
20. Wang, C., et al., *Development of a novel biodegradable and anti-bacterial polyurethane coating for biomedical magnesium rods.* Materials Science and Engineering: C, 2019. **99**: p. 344-356.
21. Chen, Z., et al., *Osteoimmunomodulatory properties of magnesium scaffolds coated with β-tricalcium phosphate.* Biomaterials, 2014. **35**(30): p. 8553-8565.
22. Ma, J., et al., *Similarities and differences in coatings for magnesium-based stents and orthopaedic implants.* Journal of Orthopaedic Translation, 2014. **2**(3): p. 118-130.
23. Masato, T., et al., *Corrosion Protection of Mg-Li Alloy by Plasma Thermal Spraying of Aluminum.* Plasma Processes and Polymers, 2007. **4**(1): p. S593-S596.
24. Julmi, S., et al., *Processing and coating of open-pored absorbable magnesium-based bone implants.* Materials Science and Engineering: C, 2019. **98**: p. 1073-1086.
25. Nastassja, L., C. Vicki, and D. Rebekah, *Cytotoxicity of Nanoparticles.* Small, 2008. **4**(1): p. 26-49.
26. Li, J., et al., *Gold nanoparticle size and shape influence on osteogenesis of mesenchymal stem cells.* Nanoscale, 2016. **8**(15): p. 7992-8007.
27. Woodruff, M.A. and D.W. Hutmacher, *The return of a forgotten polymer—Polycaprolactone in the 21st century.* Progress in Polymer Science, 2010. **35**(10): p. 1217-1256.
28. González-García, D.M., et al., *Synthesis and in Vitro Cytocompatibility of Segmented Poly(Ester-Urethane)s and Poly(Ester-Urea-Urethane)s for Bone Tissue Engineering.* 2018. **10**(9): p. 991.
29. Shrestha, B.K., et al., *Bio-inspired hybrid scaffold of zinc oxide-functionalized multi-wall carbon nanotubes reinforced polyurethane nanofibers for bone tissue engineering.* Materials & Design, 2017. **133**: p. 69-81.
30. Bhattarai, D.P., et al., *A controlled surface geometry of polyaniline doped titania nanotubes biointerface for accelerating MC3T3-E1 cells growth in bone tissue engineering.* Chemical Engineering Journal, 2018. **350**: p. 57-68.
31. Peng, F., et al., *Enhanced Corrosion Resistance and Biocompatibility of Magnesium Alloy by Mg–Al-Layered Double Hydroxide.* ACS Applied Materials & Interfaces, 2016. **8**(51): p. 35033-35044.
32. Shrestha, B.K., et al., *π-Conjugated polyaniline-assisted flexible titania nanotubes with controlled surface morphology as regenerative medicine in nerve cell growth.* Chemical Engineering Journal, 2019. **360**: p. 701-713.
33. Shrestha, S., et al., *Electrodeless coating polypyrrole on chitosan grafted polyurethane with functionalized multiwall carbon nanotubes electrospun scaffold for nerve tissue engineering.* Carbon, 2018. **136**: p. 430-443.
34. Viyannalage, L., et al., *From Grignard's reagents to well-defined Mg nanostructures: distinctive electrochemical and solution reduction routes.* Chemical Communications, 2012. **48**(42): p. 5169-5171.
35. Gribov, E.N., et al., *Vibrational and Thermodynamic Properties of H2 Adsorbed on MgO in the 300−20 K Interval.* The Journal of Physical Chemistry B, 2004. **108**(41): p. 16174-16186.
36. Sk, M.M. and C.Y. Yue, *Synthesis of polyaniline nanotubes using the self-assembly behavior of vitamin C: a mechanistic study and application in electrochemical supercapacitors.* Journal of Materials Chemistry A, 2014. **2**(8): p. 2830-2838.
37. Krimm, S. and J. Bandekar, *Vibrational Spectroscopy and Conformation of Peptides, Polypeptides, and Proteins*, in *Advances in Protein Chemistry*, C.B. Anfinsen, J.T. Edsall, and F.M. Richards, Editors. 1986, Academic Press. p. 181-364.
38. Gao, R., et al., *Fabrication of fibrous szaibelyite with hierarchical structure superhydrophobic coating on AZ31 magnesium alloy for corrosion protection.* Chemical Engineering Journal, 2014. **241**: p. 352-359.

39. Liu, W., et al., *Physical–chemical stability and in vitro digestibility of hybrid nanoparticles based on the layer-by-layer assembly of lactoferrin and BSA on liposomes.* Food & Function, 2017. **8**(4): p. 1688-1697.
40. Chen, Y., et al., *Sandwiched polydopamine (PDA) layer for titanium dioxide (TiO2) coating on magnesium to enhance corrosion protection.* Corrosion Science, 2015. **96**: p. 67-73.
41. Zhang, W., et al., *Strengthened corrosion control of poly (lactic acid) (PLA) and poly (ε-caprolactone) (PCL) polymer-coated magnesium by imbedded hydrophobic stearic acid (SA) thin layer.* Corrosion Science, 2016. **112**: p. 327-337.
42. Zhao, D., et al., *Current status on clinical applications of magnesium-based orthopaedic implants: A review from clinical translational perspective.* Biomaterials, 2017. **112**: p. 287-302.
43. Omanovic, S. and S.G. Roscoe, *Electrochemical Studies of the Adsorption Behavior of Bovine Serum Albumin on Stainless Steel.* Langmuir, 1999. **15**(23): p. 8315-8321.
44. Qin, H., et al., *Enhanced antibacterial properties, biocompatibility, and corrosion resistance of degradable Mg-Nd-Zn-Zr alloy.* Biomaterials, 2015. **53**: p. 211-220.
45. MacDonell, R., M.W. Hamrick, and C.M. Isales, *Protein/amino-acid modulation of bone cell function.* BoneKEy reports, 2016. **5**: p. 827-827.

**Figures and captions**

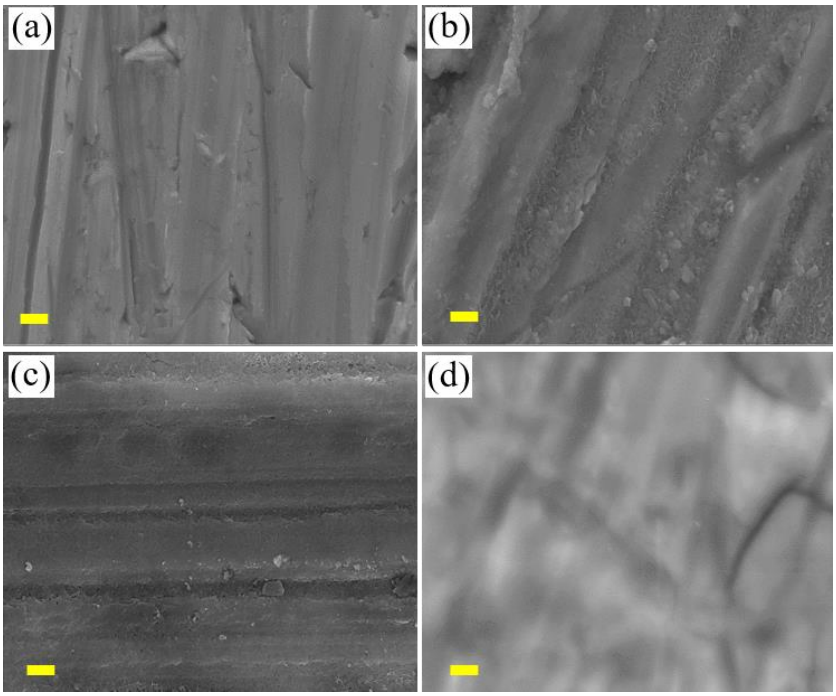


Fig. 1. FE-SEM images showing surface microtopography of (a) pure Mg, (b) Mg-OH, (c) Mg-OH-AA, and (d) Mg-OH-AA-BSA before treated in SBF solution at 37 °C for the evaluation of potentiodynamic polarization parameters. (The scale bar =2 μm).

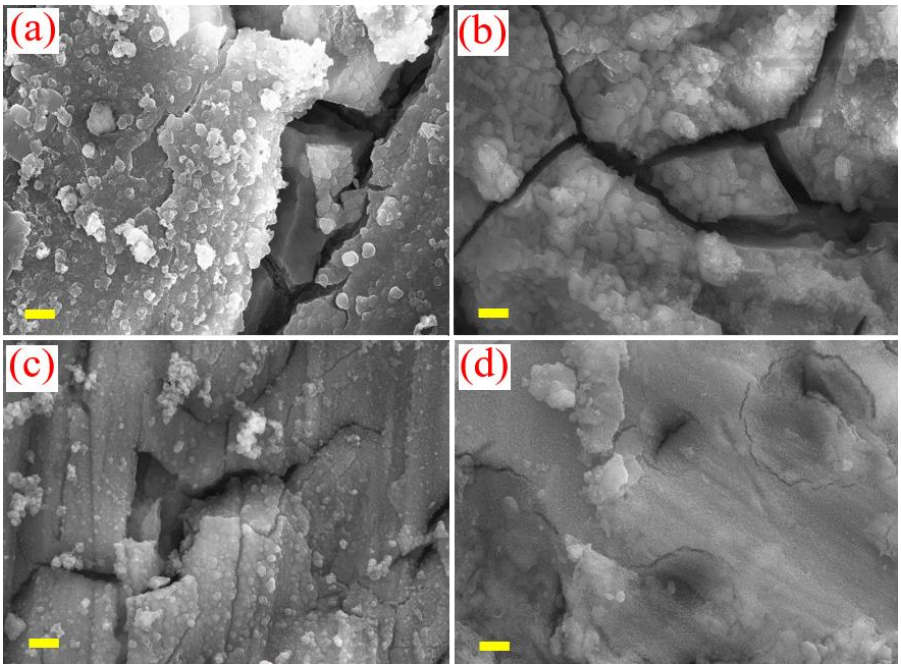


Fig. 2. Representative FE-SEM surface morphology of (a) pure Mg, (b) Mg-OH, (c) Mg-OH-AA, and (d) Mg-OH-AA-BSA after potentiodynamic polarization test conducted on SBF solution at 37 °C. (The scale bar =1 μm).

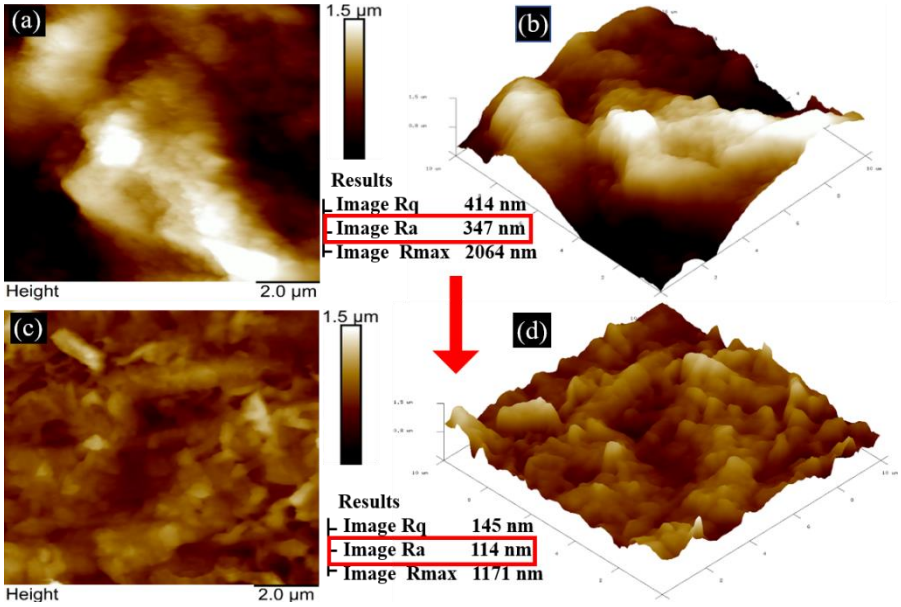


Fig. 3. Atomic force microscopy images in 2D and 3D forms of pure Mg (a and b), and Mg-OH-AA-BSA (c and d) after polarization test in (SBF) at 37 °C.

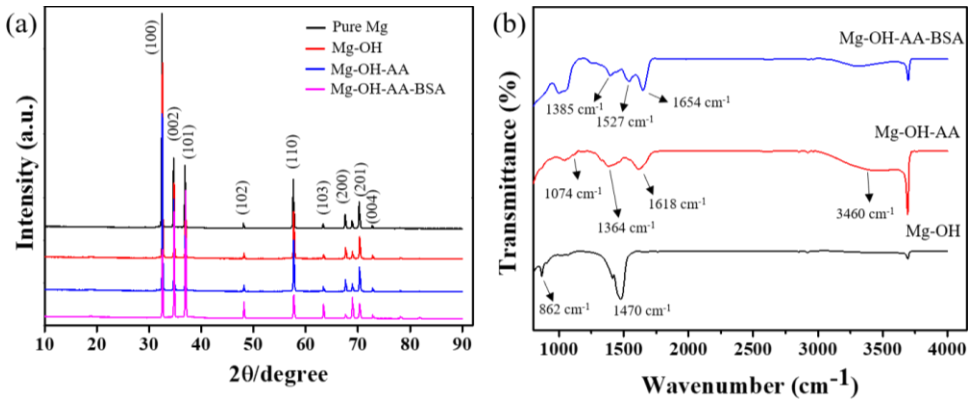


Fig. 4. (a) XRD analysis of pure Mg and other surface modified Mg samples. (b) FT-IR spectra of as-prepared samples surface.

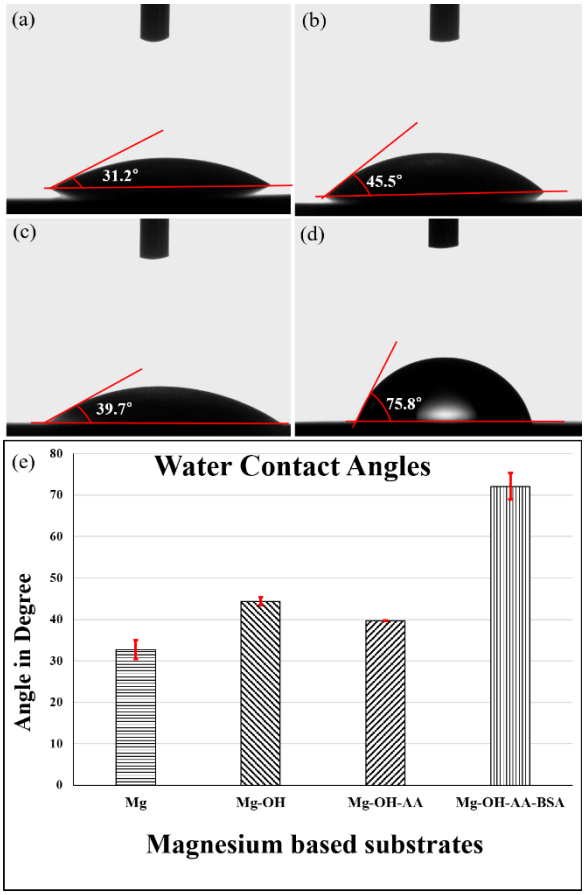


Fig. 5. Water contact angle values of the samples including (a) pure Mg, (b) Mg-OH, (c) Mg-OH-AA, and (d) Mg-OH-AA-BSA at room temperature. The WAC value of each sample was obtained before potentiodynamic corrosion measurements.

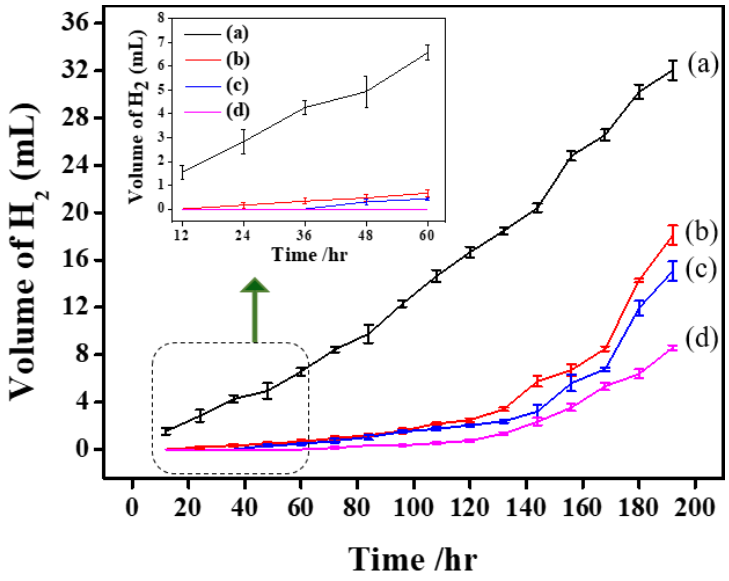


Fig. 6. (a) Hydrogen evolution evaluation (a) pure Mg, (b) Mg-OH, (c) Mg-OH-AA, (d) Mg-OH-AA-BSA substrate. (n=3).

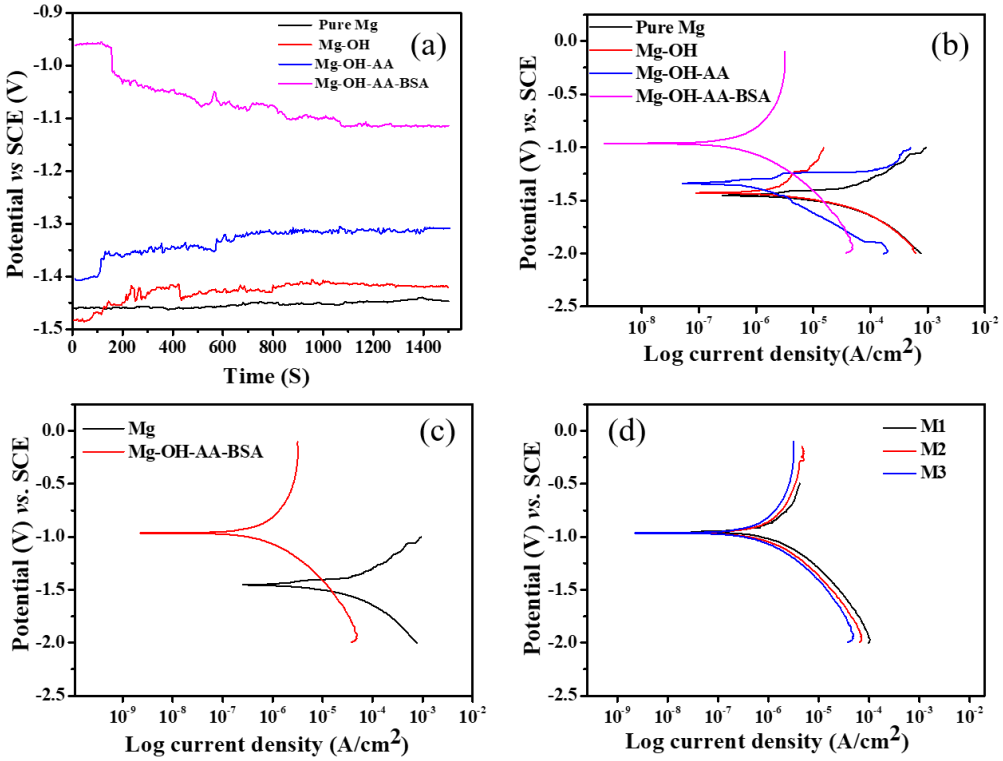


Fig. 7. Electrochemical corrosion study. (a) OCP vs. time; (b) potentiodynamic polarization curves; (c) potentiodynamic polarization curves of Mg and Mg-OH-AA-BSA only; and (d) polarization curves obtained from Mg-OH-AA-BSA(n=3). All samples were treated in SBF solution at 37 °C for 1 h 30 min before analytical measurements.

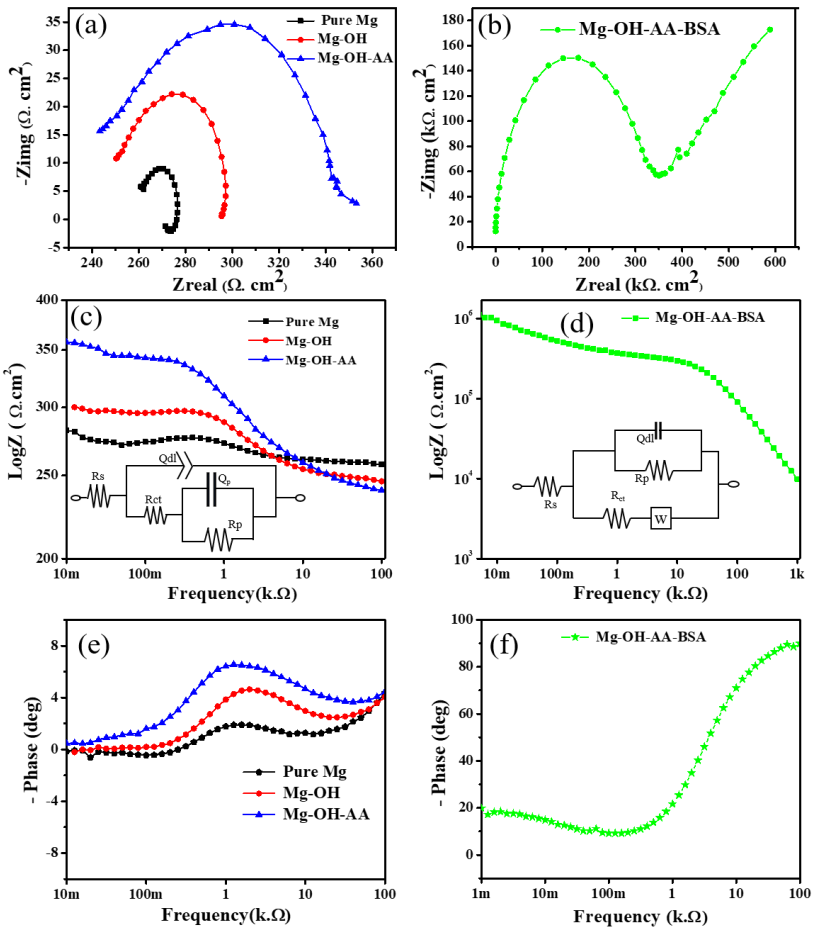


Fig. 8. Electrochemical impedance spectroscopy analysis. (a and b) Nyquist plots and (c-f) bode plots of the samples measured on SBF solution at 37 ℃. (insets Figs. in (c) and (d) represent the equivalent electrical circuit of EIS spectra obtained from Fig a and b respectively.

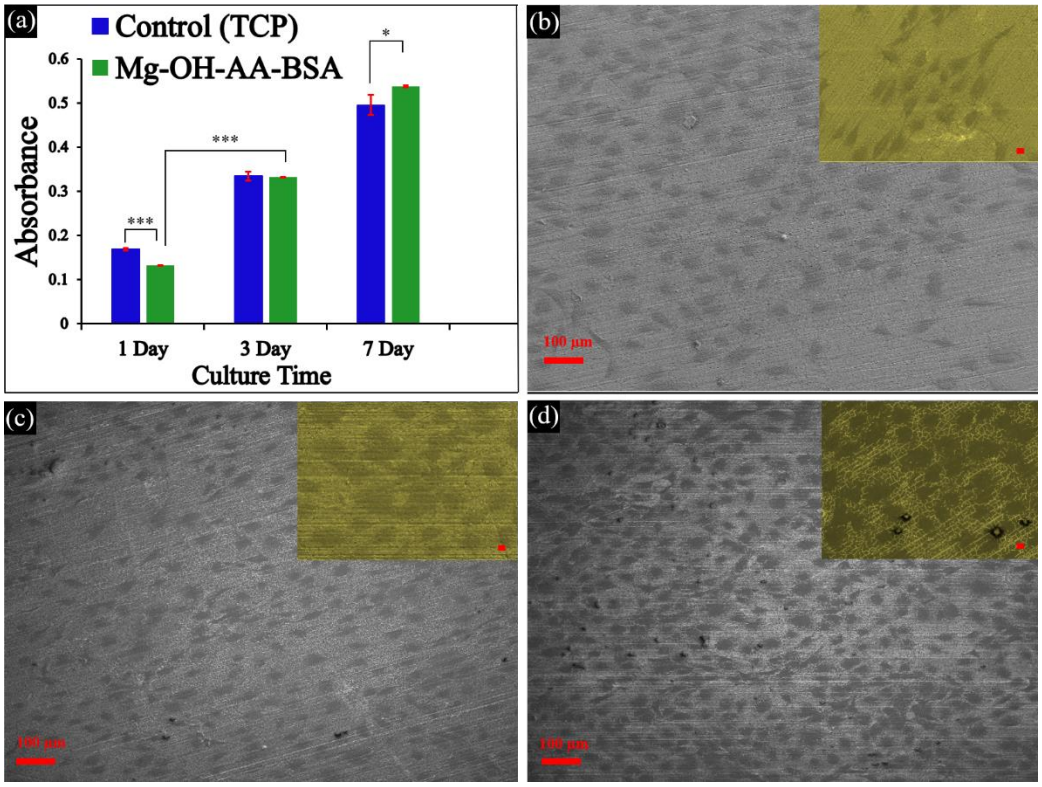


Fig. 9. (a) Pre-osteoblast cell viability (cell counting Kit-8, CCK8 test) on the Mg-OH-AA-BSA (samples) and TCP (as control). Representative SEM images of MC3T3-E1 cells cultured on Mg-OH-AA-BSA scaffolds surface after 1, 3, and 5 days of culture. Data presented as mean ± SD and analyzed using an ANOVA, *$p < 0.05$, and ***$p < 0.001$ (The scale bar =20 µm (insets figs).

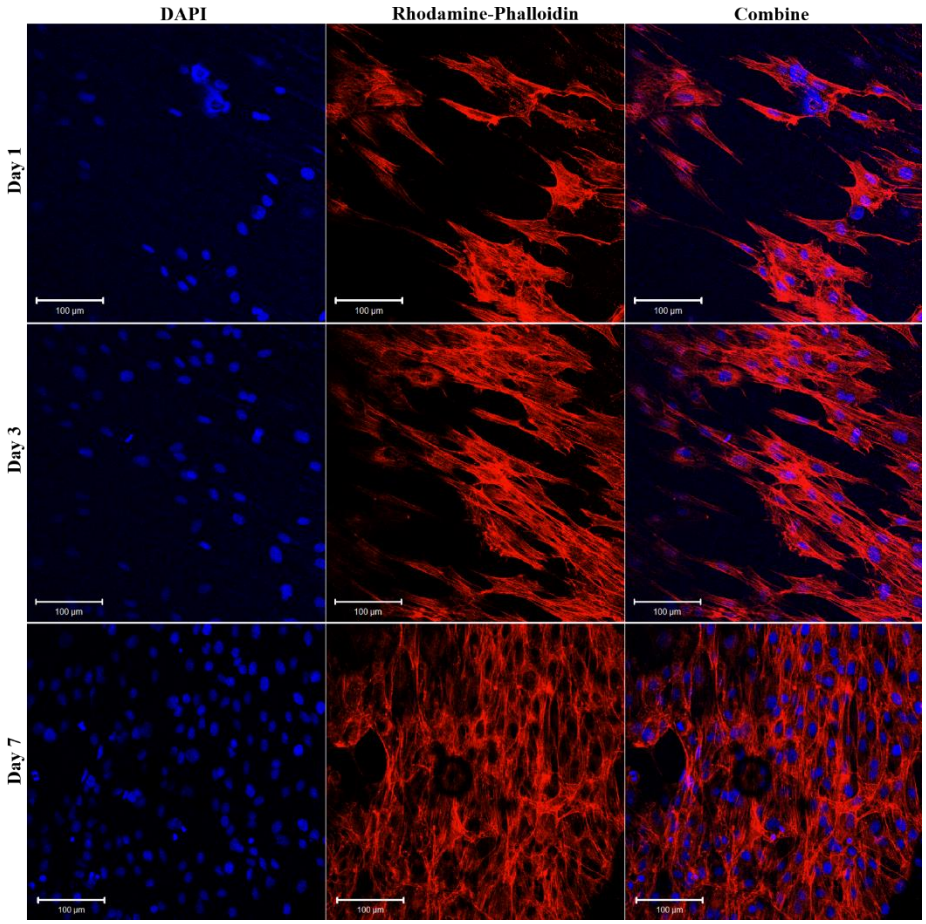


Fig. 10. Fluorescence images of MC3T3-E1 pre-osteoblast cells attached on Mg-OH-AA-BSA scaffolds. The cells were cultured on the samples for 1 day, 3 days and 7 days separately. Nuclei and cytoplasm were stained by DAPI (blue) and Rhodamine- Phalloidin (red) respectively. (scale bar =100 μm).

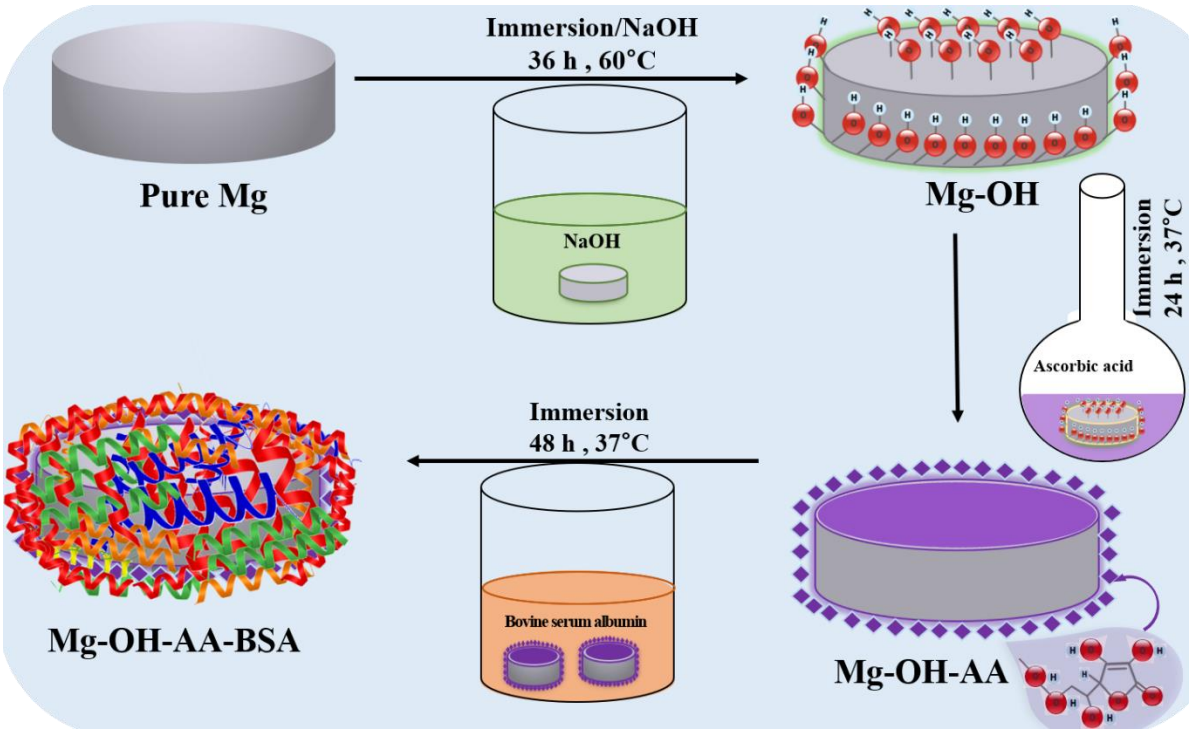


Schematic 1. A diagrammatic representation of the modification on pure Mg surface via layer-by-layer formation of chemical bonds into Mg-OH-AA-BSA for enhancing anti-corrosion and osteo-inductive property.